Microelectronics Reliability 110 (2020) 113656

Contents lists available at ScienceDirect

Microelectronics Reliability

journal homepage: www.elsevier.com/locate/microrel

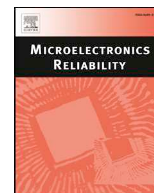

High-energy proton irradiation effects on GaN hybrid-drain-embedded gate injection transistors

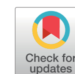

Alessandro Floriduz*, James D. Devine

Electrical Network Projects Section, Electrical Group, Engineering Department, CERN, CH-1211 Geneva 23, Switzerland

ARTICLE INFO

Keywords:
Proton irradiation effects
GaN
HEMT
Hybrid-drain-embedded gate injection transistors
LED power supply

ABSTRACT

The characterization of commercial-grade power transistors upon high levels of particle irradiation is required to enable radiation tolerant LED power supplies for the new luminaires of CERN accelerator tunnels, which represent a harsh environment for semiconductor devices. This work describes the effects of 24 GeV/c proton irradiation on commercial GaN hybrid-drain-embedded gate injection transistors (HD-GITs) after a fluence of 5.9×10^{14} p/cm^2. Measurements of drain leakage current, threshold voltage and $I_{ds} - V_{ds}$ curves show that only a minor variation occurs in the electrical properties of GaN HD-GITs after the considered fluence; for example, an average increase of ≈11–13 mV is found in the threshold voltage upon irradiation. We also put forward a physical explanation of the observed degradation caused by proton irradiation; in particular, the electron drift velocity in the 2DEG channel at high electric fields appears to decrease due to a radiation-induced increase in phonon relaxation rate. Finally, an AC/DC LED power supply with current control using GaN HD-GITs is proposed for the new luminaires of CERN tunnels, meeting the requirements in terms of radiation hardness and light quality.

1. Introduction

CERN accelerator tunnels constitute a very harsh environment, where the yearly radiation levels on tunnel walls can exceed 1 kGy(Si) of absorbed dose and a 1 MeV neutron equivalent (neq) fluence in silicon of 5×10^{12} n/cm^2 [1]. Development of rad-hard LED luminaires for CERN tunnels is required to cope with the obsolescence of traditional fluorescent lamps with magnetic ballast. Commercial white GaN LEDs have been recently irradiated with 24 GeV/c protons [2] and it was found that, at a typical drive current of 200 mA, a 50% degradation in light output occurs after a fluence of 4×10^{13} p/cm^2 (corresponding to a 1 MeV neq fluence in Si of 2.3×10^{13} n/cm^2) which also deposited ≈11 kGy(Si) of ionizing energy in the irradiated LEDs. These levels correspond to > 5 years of radiation exposure in the typical section of CERN tunnel walls, thus validating the use of white LEDs as light source in rad-hard luminaires. Based on these results, all other components comprised in such rad-hard LED-based lights shall present no degradation at a 1 MeV neq fluence in Si of 2.3×10^{13} n/cm^2 and an absorbed dose of 11 kGy(Si). Commercial-grade optical materials exhibiting no or negligible reduction in light transmission after these radiation levels have been recently identified [3]. However, no commercial LED power supply will be able to withstand the target radiation levels [4]. A rad-hard LED power supply, based on a simple diode bridge rectifier, has been implemented in custom-designed LED emergency lights which are now being installed in CERN accelerator complex [4], however the same principle cannot be adopted in luminaires for general lighting having higher power rating (> 30 W), as it would provide insufficient tolerance to mains voltage variations and poor LED current regulation, leading to light flickering. The AC/DC passive LED power supply described in [5], which can be radiation hardened by use of SiC Schottky diodes, is also unsuitable because of the activation of its bulky inductors, posing problems from a radiation safety viewpoint. Therefore an AC/DC power supply with current control capable of withstanding the target radiation levels (2.3×10^{13} n/cm^2 and 11 kGy) has to be designed. In particular, cost-effective power transistors rated ≥500 V meeting our requirements in terms of radiation tolerance have to be identified. Commercial Si and SiC MOSFETs cannot be used as they fail after a few kGy(Si) [6,7]. Rad-hard Si MOSFETs can present as well a degradation in their characteristics at the target levels [6] and their high cost is not compatible with budget constraints. On the other hand, depletion-mode AlGaN/GaN high electron mobility transistors (HEMTs) offer a much higher radiation tolerance than conventional Si and GaAs transistors [8], however use of normally-ON transistors in power electronics applications is cumbersome, as they require more complicated control circuitries than normally-OFF devices.

In recent years, normally-OFF AlGaN/GaN HEMTs grown on Si

* Corresponding author.
E-mail address: alessandro.floriduz@alumni.cern (A. Floriduz).

https://doi.org/10.1016/j.microrel.2020.113656
Received 23 August 2019; Received in revised form 23 December 2019; Accepted 6 April 2020
Available online 29 May 2020
0026-2714/ © 2020 The Authors. Published by Elsevier Ltd. This is an open access article under the CC BY license (http://creativecommons.org/licenses/BY/4.0/).

substrate have appeared on the market. Different solutions are adopted in commercial products to achieve normally-OFF operation of AlGaN/GaN HEMTs: for example, Transphorm utilizes the cascode of an insulated-gate depletion-mode AlGaN/GaN HEMT with a low-voltage (LV) Si MOSFET [9]; in Texas Instruments 600 V GaN-based products [10], a depletion-mode AlGaN/GaN HEMT is connected in series with a LV Si MOSFET with the gates of the two transistors controlled separately by a Si ASIC driver unit integrated in the device package; in Sanken products, normally-OFF behaviour is achieved by use of a recessed gate with a NiO_x/Ni/Au electrode, in which NiO_x acts as a p-type material [11]; in EPC [12], GaN Systems [13] and Navitas [14] products, normally-OFF operation is obtained through a non-recessed p-GaN gate; finally, Panasonic introduced hybrid-drain-embedded gate injection transistors (HD-GITs), in which normally-OFF operation is achieved through a recessed p-GaN gate with an ohmic contact on the p-GaN layer [15]; HD-GITs also present a non-recessed p-GaN layer close to the drain contact, electrically connected to it, which injects holes during OFF-state so as to mitigate current collapse [15].

Over the past years, both research-grade (like e.g. [16,17]) and commercial normally-OFF AlGaN/GaN HEMTs have been tested against irradiation; in particular, commercial devices from Transphorm [18], EPC (see e.g. [12,19–24]), GaN Systems [24–29], and Panasonic [25–30] have been tested and studied. These works showed that normally-OFF commercial AlGaN/GaN HEMTs, in the same manner as their depletion-mode counterparts, exhibit a very high resistance to displacement damage and ionizing effects, far exceeding that of commercial Si and SiC MOSFETs. In particular, Hommels et al. have recently tested Panasonic HD-GITs and GaN Systems HEMTs against very high levels of particle irradiation (such as a fluence of 5.8×10^{15} p/cm^2 of 600 MeV protons) [26,27] and obtained very promising results, with the devices showing only limited degradation after these radiation levels; in addition, they found that HD-GITs exhibited more consistency in their characteristics upon irradiation with respect to GaN Systems HEMTs [27]. Moreover, HD-GITs have also been recently tested by Mizuta et al. [30], and showed a great robustness against single event effects (SEEs). Based on the results obtained in [26,27,30], and given the lack of other previous reports on displacement damage of commercial devices with voltage rating $\geq$600 V (reports [18,24,25,28] are focused on SEE testing, and [29] describes only low-dose γ-ray irradiation), we selected Panasonic HD-GITs as potential candidate transistors for rad-hard LED power supplies. Notwithstanding the encouraging results from Hommels et al., it remains important to characterize HD-GITs at fluences lower than those reached in [26,27] and comparable to those expected after a multi-year radiation exposure on the tunnel walls of a typical section of CERN accelerators, in order to quantify the amount of radiation damage after a fluence more similar but still sufficiently higher than our minimum target value of 2.3×10^{13} n/cm^2. This is indeed required to verify if, at the expected radiation levels, HD-GITs are still essentially unaffected or if they already exhibit a small (but non-negligible) amount of damage. For example, Hommels et al. [26] found that the threshold voltage of HD-GITs increased by $\approx$0.2 V after a 300 MeV pion fluence of 10^{15} π/cm^2; if the transistors were to be operated in semi-ON condition (and, as it will be detailed further below, this is exactly the operation mode of HD-GITs in our proposed rad-hard LED power supply), such threshold voltage shift would already impact significantly the behaviour of the power supply in which these devices are used. Therefore, knowledge of upper bound limits of radiation damage is in general not enough to properly design a rad-hard power supply and to select its components; a better understanding of radiation effects around the target levels is indeed required. Since the interpolation of irradiation data of devices from different manufacturers would lead to uncertain results (due to the differences in technologies and device structures, as detailed above), a dedicated irradiation campaign of HD-GITs at moderate radiation levels is necessary.

This work presents the degradation of electrical characteristics of Panasonic PGA26E19BA and PGA26E07BA HD-GITs upon irradiation with 24 GeV/c protons at a fluence of 5.9×10^{14} p/cm^2. Apart from describing for the first time the effects of high-energy protons on HD-GITs at a moderate fluence, we also postulate a physical explanation, not addressed in the previous publications on HD-GITs [25–30], of the observed degradation in drain leakage current, threshold voltage and output $I_{ds} - V_{ds}$ characteristics. Finally, we propose a rad-hard LED power supply with current control using HD-GITs, that can be implemented in radiation tolerant luminaires for CERN accelerator tunnels.

This report is organized as follows: Section 2 provides the experimental details; Section 3 illustrates the electrical characteristics of irradiated devices. The proposed rad-had LED power supply is described in Section 4, and Section 5 is devoted to the conclusions.

2. Experimental details

2.1. Devices under test

The enhancement-mode AlGaN/GaN transistors under test are hybrid-drain-embedded gate injection transistors (HD-GITs) from Panasonic. Information on the HD-GIT structure (whose schematic cross-section is illustrated in Fig. 1) can be found in [15,31–35]. The devices are grown on 6-inch wafers of p-doped Si(111) by metal organic chemical vapour deposition. From bottom to top, the structure comprises: *i*) a nucleation layer (NL) with an AlGaN layer on the top of an AlN layer; *ii*) an AlN/GaN superlattice strain relief layer (SRL), to effectively relax the epitaxial strain due to lattice mismatch, so as to improve crystal quality and reduce threading dislocation density; *iii*) a semi-insulating GaN (i-GaN) layer, on the top of which a semi-insulating AlGaN (i-AlGaN) barrier is grown. The piezoelectric and spontaneous polarization fields at the AlGaN/GaN heterostructure induce a 2DEG in the i-GaN layer. Normally-OFF operation is achieved through a recessed p-GaN gate. Carbon doping is used to achieve semi-insulating GaN layers, so as to obtain devices with high breakdown voltage and low leakage current. However, the deep acceptor states introduced by carbon ions in these layers induce current collapse, i.e. an increase in the dynamic R_{on} due to hole emission in the epilayer around the drain region during OFF-state at high V_{ds}. In HD-GITs, current collapse is suppressed by the introduction of a non-recessed p-GaN drain (hereafter p-drain), electrically connected to the drain electrode, which injects holes during OFF-state operation, thus compensating the aforementioned hole emission from deep traps in OFF-state at high V_{ds}. This growth and process technology is implemented in the commercial devices under test: Panasonic PGA26E19BA and PGA26E07BA HD-GITs, which present a maximum R_{on} of, respectively, 190 mΩ and 70 mΩ at a junction temperature of 25 °C.

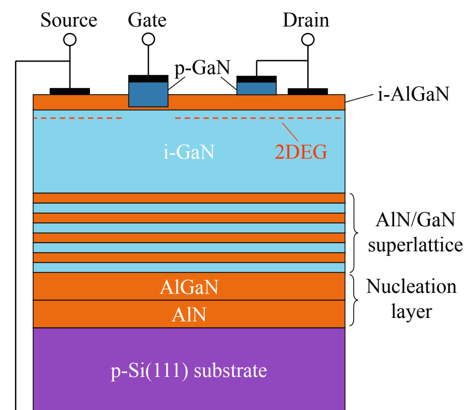

Fig. 1. Schematic cross-section of a GaN-based HD-GIT (not to scale).

2.2. Irradiation conditions and measurement setup

Three samples of both PGA26E07BA and PGA26E19BA HD-GITs (hereafter denoted as E07 and E19, respectively) were irradiated at IRRAD facility at CERN [36], using a 24 GeV/c proton beam. For irradiation purposes, each HD-GIT (in a DFN8X8 package) was mounted on a 5 × 5 cm^2 sample holder made of cardboard, installed on an irradiation table in IRRAD. Irradiation was done at atmospheric pressure and room temperature, with the devices in OFF condition and with their contact pads floating. This irradiation condition is representative of the actual application of HD-GITs as transistors for power supplies in rad-hard LED lights, since these lights and hence their power supplies need to be turned on only when access by human operators to the accelerator tunnels is possible, and this access can be permitted only when the accelerator itself (i.e. the source of radiation) is switched off; this means that power supply components will not be irradiated while they are in ON state, as irradiation will occur only when the accelerator is operating and human access to the tunnel is prohibited, during which time the lights are extinguished. The impinging proton beam has a nominal Gaussian profile of 1.2 × 1.2 cm^2 (FWHM). The bunches composing the irradiating beam were spaced enough so that heating of HD-GIT samples due to proton bombardment was negligible. Irradiation of the six samples lasted 79 h. The fluence reached at the end of the irradiation is 5.9×10^{14} p/cm^2. This 24 GeV/c proton fluence corresponds to a 1 MeV neq fluence in Si of 3.4×10^{14} n/cm^2; the experimental non-ionizing energy loss hardness factor is used as conversion factor from 24 GeV/c proton fluence into 1 MeV neq fluence in Si, and is equal to 0.58 [37]. This fluence corresponds to > 20 years of radiation exposure on the walls of a typical section of CERN accelerator tunnels [1]. In addition, the absorbed dose in GaN HD-GITs corresponding to the achieved fluence of 24 GeV/c protons is ≈157 kGy(Si) (the fluence to dose equivalent conversion factor for 24 GeV/c protons is 2.67×10^{-10} Gy(Si) × cm^2/p [38]).

Measurements were taken after a cool-down period of 10 days, when the residual activation of the samples became acceptably low (≲20 μSv/h at contact). During the cool-down period, samples were stored at room temperature. We speculate that only marginal recovery (if any) occurred in our samples during the cool-down period, in view of the significant thermal stability of defects produced in GaN by high fluence particle irradiation [39]. Results available in literature seem to support our conjecture: for example, no recovery in electrical characteristics after annealing at room temperature for several weeks was detected in previous reports on proton-irradiated AlGaN/GaN HEMTs [40,41]; nevertheless, we cannot exclude that some form of recovery (associated to unstable radiation-induced defects) actually took place in our samples during the cool-down period.

For each sample, the following quantities have been measured before and after irradiation: *i*) the drain leakage current I_{dss}, obtained at V_{gs} = 0 V and V_{ds} = 600 V; *ii*) the transfer $I_{ds} - V_{gs}$ characteristics, measured with V_{ds} = 10 V; *iii*) the output $I_{ds} - V_{ds}$ characteristics, measured at different values of V_{gs}. Two Keithley 2410 source-meter units were used to perform the electrical measurements. All measurements, before and after irradiation, have been taken at a chuck temperature of 35 °C; this temperature was chosen to prevent condensation of air moisture on the devices under test, which could have formed due to uncontrolled humidity within the room where the probe station was located.

3. Results and discussion

3.1. Drain leakage current

We now present the evolution of electrical characteristics of E19 and E07 HD-GITs with proton exposure, by starting with the analysis of the variations in drain leakage current I_{dss}. The experimental analysis of leakage current in HD-GITs has been recently reported by Tanaka et al. in [35], where it is shown that I_{dss} predominantly flows from the p-drain to the substrate and mostly consists in recombination current of injected holes and electrons from the 2DEG beneath the p-drain. Previous studies on AlGaN/GaN HEMTs grown on Si substrate with an undoped GaN buffer on AlN/GaN/AlN NL or with a weakly p-type GaN buffer (and undoped channel region) on SRL have shown that current conduction from the GaN buffer to the substrate through the intermediate layers (SRLs or NLs) occurs via thermally assisted multistep tunnelling, hopping, and Poole-Frenkel emission [42,43]. In particular, recent studies on full vertical stacks (AlGaN/GaN/SRL/NL/p-Si) and on AlN/p-Si structures have identified the following leakage paths: *i*) defect-assisted multistep band-to-band tunnelling [44] of electrons from the valence band of the i-GaN layer to the 2DEG [45,46]; *ii*) leakage of electrons from the p-Si substrate through the AlN layer via hopping, Poole-Frenkel conduction, Fowler-Nordheim tunnelling and trap-assisted tunnelling [47–50]. We assume that these mechanisms are also responsible for the vertical leakage current observed in HD-GITs (which have an i-GaN layer on AlN/GaN superlattice SRL and AlGaN/AlN NL, cf. Section 2.1).

The values of I_{dss} before and after irradiation of E19 and E07 HD-GITs are collected in Table 1. I_{dss} increases on average by 0.1 μA and 0.34 μA in E19 and E07 samples, respectively. We propose the following interpretation of the increase in I_{dss}: proton irradiation introduces a wide range of defects in the AlGaN/GaN heteroepitaxial structure and in the buffer layer, namely vacancies and interstitials of Al, N, and Ga atoms and complexes thereof with each other, with pre-existing defects and with growth impurities and dopants [8,39,51], thus increasing the trap density throughout all device layers. The current density for both hopping [52] and thermally assisted multistep tunnelling [53,54] is dependent on the trap concentration and, consequently, the radiation-induced increase of defect density leads to an increase in I_{dss}. In addition, also Poole-Frenkel conduction increases upon irradiation, as long as radiation-induced defects do not compensate each other or pre-existing traps [55]. In addition, unlike high-temperature reverse bias tests on HD-GITs [35], the increase in I_{dss} upon irradiation is not correlated to its initial value. In any case, the values are always well below the maximum specified in the datasheets at 25 °C [56,57]. As a concluding remark, we note that a radiation-induced increase in I_{dss} was also obtained by Hommels et al. on Panasonic GaN HD-GITs [26]; as in our measurements, the values of I_{dss} after irradiation were still within limits despite the use of even higher fluences.

3.2. Threshold voltage

Let us now discuss the effects of proton irradiation on the transfer characteristic and threshold voltage of GaN HD-GITs. Fig. 2a and b illustrate the transfer $I_{ds} - V_{gs}$ curves of E19 and E07 transistors, respectively. Equivalent results were obtained for all HD-GITs of the same variant, so only one representative curve per type is shown. As can be seen for both variants, the transfer characteristics after 5.9×10^{14} p/cm^2 present only very small changes with respect to the curves before irradiation. This behaviour illustrates the higher robustness of GaN HD-GITs against displacement damage and dose effects with respect to Si and SiC power MOSFETs (see e.g. [6,7]). In particular, the $I_{ds} - V_{gs}$

Table 1
I_{dss} before and after irradiation of E19 and E07 samples.

Sample	I_{dss} before	I_{dss} after	ΔI_{dss}	Relative variation
E19–01	0.408 μA	0.546 μA	+0.138 μA	+33.8%
E19–02	0.407 μA	0.494 μA	+0.087 μA	+21.4%
E19–03	0.487 μA	0.565 μA	+0.078 μA	+16.0%
E07–01	1.096 μA	1.251 μA	+0.155 μA	+14.1%
E07–02	1.124 μA	1.416 μA	+0.292 μA	+26.0%
E07–03	1.023 μA	1.584 μA	+0.561 μA	+54.8%

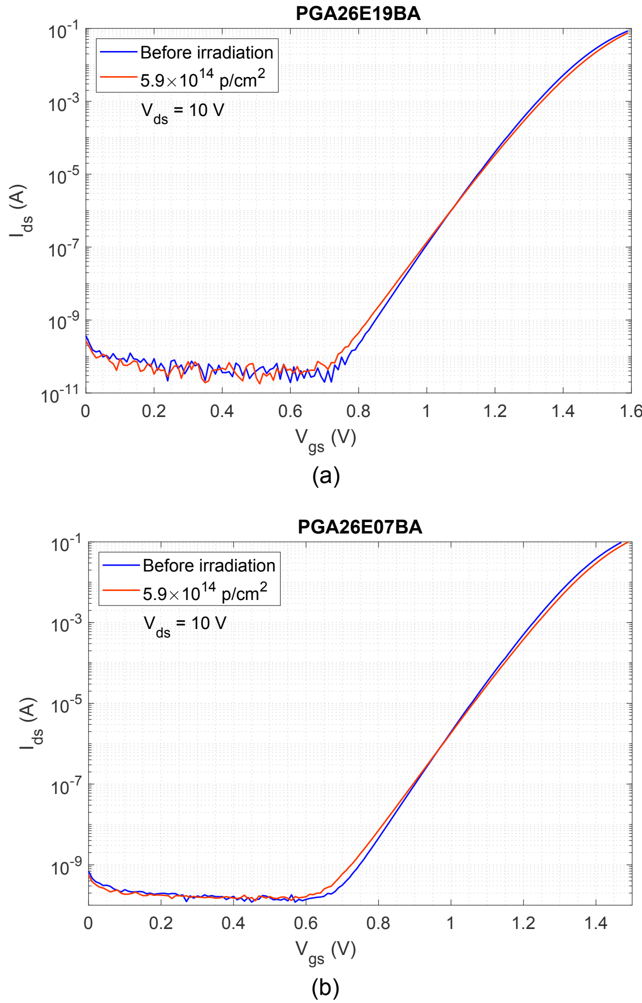

Fig. 2. $I_{ds} - V_{gs}$ curves of (a) PGA26E19BA and (b) PGA26E07BA samples before and after irradiation, with V_{ds} = 10 V.

curves after irradiation exhibit a very small shift towards positive voltages and an increase in drain current at low values of V_{gs} (when the transistors are in cut-off condition). We attribute this increase in I_{ds} at low V_{gs} to radiation-induced increase in trap density, thus enhancing current leakage mechanisms as described in Section 3.1. The shift of $I_{ds} - V_{gs}$ curves towards positive values observed after irradiation for $V_{gs} \gtrsim 1$ V induces a small variation in the threshold voltage, and its origin is discussed later in this Section. As a combination of these two effects (the increase in I_{ds} at low V_{gs} and the shift of $I_{ds} - V_{gs}$ curves to positive voltages), the subthreshold slope is seen to change upon irradiation, particularly for $I_{ds} < 10^{-4}$ A.

The values of threshold voltage V_{th} were extracted from $I_{ds} - V_{gs}$ characteristics. For reasons of consistency, V_{th} was defined as in the product manufacturer's datasheets [56,57]: for E19 samples, V_{th} is computed as the V_{gs} at which I_{ds} = 1 mA at V_{ds} = 10 V; for E07 samples, V_{th} is computed as the V_{gs} at which I_{ds} = 2.6 mA at V_{ds} = 10 V. The values of V_{th} before and after irradiation of E19 and E07 samples are collected in Table 2. V_{th} increases on average by 10.6 mV and 13 mV upon irradiation in E19 and E07 samples, respectively. ΔV_{th} seems to be anti-correlated to the value of V_{th} before irradiation, but we cannot draw definitive conclusions due to limited sample size. This trend will be further investigated in future studies. The small variations in V_{th} we observed upon irradiation (Table 2) are within the statistical manufacturing spread of GaN HD-GITs (see e.g. [33]), and do not have any impact from a practical viewpoint.

We attribute the increase in V_{th} to negatively charged traps induced by radiation. Different types of acceptor-like defects can be introduced in AlGaN/GaN heterostructures by proton irradiation. For example, in [58] the positive shift of V_{th} of AlGaN/GaN heterojunction Schottky diodes is attributed to a radiation-induced acceptor state at $E_C - 3.25$ eV in the undoped GaN layer. Puzyrev et al. [59], through quantum molecular dynamics calculations, attributed the positive V_{th} shift to radiation-induced N interstitials, Ga–N divacancies, and Ga vacancies, behaving as acceptor-like traps, formed in the AlGaN barrier from pre-existing Ga vacancies and N antisites. Moreover, Roy et al. [40] claimed that also radiation-induced N vacancies in the AlGaN barrier behave as acceptors and hence contribute to shifting V_{th} towards positive values.

Table 2
V_{th} before and after irradiation of E19 and E07 samples.

Sample	V_{th} before	V_{th} after	ΔV_{th}	Relative variation
E19–01	1.311 V	1.328 V	+17 mV	+1.30%
E19–02	1.326 V	1.336 V	+10 mV	+0.75%
E19–03	1.378 V	1.383 V	+5 mV	+0.36%
E07–01	1.304 V	1.311 V	+7 mV	+0.54%
E07–02	1.267 V	1.279 V	+12 mV	+0.95%
E07–03	1.154 V	1.174 V	+20 mV	+1.73%

The positive threshold voltage shift we measured is in line with the data from Hommels et al. [26], who found a positive ΔV_{th} of ≈0.2 V after a 300 MeV pion fluence of 10^{15} π/cm^2. It is also interesting to note that other commercial normally-OFF AlGaN/GaN HEMTs with p-GaN gate from EPC [12,20–23] and Freebird [19] (which implements EPC technology), as well as research-grade devices with p-AlGaN gate [16], exhibit a negative ΔV_{th}, both under proton [16,19,20,22] and γ-ray [12,21–23] irradiation. In these works, the negative ΔV_{th} was attributed to radiation-induced introduction of donor-like traps throughout the device layers [19] and hole removal in the p-type gate [16]. We believe that the different evolution of V_{th} with radiation between Panasonic HD-GITs and the devices tested in [12,16,19–23] is due to the different growth and process technology adopted, leading to different radiation-induced defects.

We would like to conclude the section with a consideration on the relation between the acceptor-like traps responsible for the positive V_{th} shift and the defects causing the I_{dss} increase discussed in Section 3.1. Acceptor-like traps, being negatively charged, would not contribute to hopping or trap-assisted tunnelling of electrons, in view of their small cross-section for electron capture [60,61]. So, if radiation introduced only acceptor-like defects in HD-GITs, then the drain leakage current increase measured experimentally would be difficult to explain. We therefore conjecture that proton irradiation introduces in GaN HD-GITs not only acceptor-like traps, but also defects with other charge states (such as N vacancies, which are donor-like traps in GaN [39]). These such defects, being neutral or positively charged, will have higher cross-sections and hence will be effective in promoting hopping and trap-assisted tunnelling of electrons [54,60,61]. So, an increase in neutral and positively charged trap density in HD-GITs will lead to an increase in I_{dss}. Although we did not perform a dedicated analysis to identify the radiation-induced traps, we believe that the proposed mechanism could be realistic. The overall V_{th} shift would then be the result of the joint effect of donor- and acceptor-like defects. We could suppose that acceptor-like defects are introduced by radiation in HD-GIT at a higher rate than donor-like traps, the V_{th} shift observed being positive. Alternatively, we could speculate that the density of acceptor-like traps generated by radiation is higher in regions of the HD-GITs where their influence on V_{th} is stronger (like e.g. in the top AlGaN layer), and that radiation-induced donor-like traps are more abundantly located in regions where their impact on the vertical leakage is higher (like e.g. in the AlN nucleation layer). Such decoupling in the spatial distribution of donor- and acceptor-like defects might be due to different defect generation dynamics in the individual layers of the vertical structure of

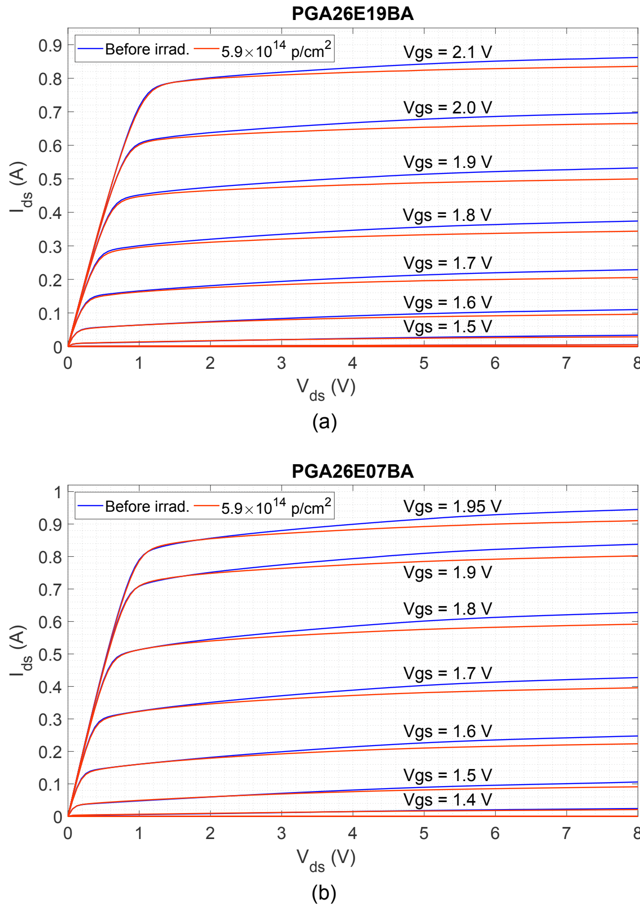

Fig. 3. $I_{ds} - V_{ds}$ curves of (a) PGA26E19BA and (b) PGA26E07BA samples before and after irradiation. The values of V_{gs} are indicated. In panels (a) and (b) are also shown, respectively, the curves with V_{gs} of 1.4 V and 1.2 V (E19), and 1.2 V (E07), which lay down close to the V_{ds} axis.

GaN HD-GITs, and would in turn lead to a decoupled behaviour upon irradiation of I_{dss} and V_{th} shift. A decoupled evolution with radiation of V_{th} and I_{dss} is also found in [17], where the effect of neutron and Xe ion irradiation on p-GaN gate HEMTs (grown on Si substrate) is studied. There, it is reported that the drain leakage current increases under Xe ion irradiation and decreases under neutron bombardment, while V_{th} shifts positively under both types of irradiation. Neutrons and heavy ions introduce different defects in GaN materials (see e.g. [8,39]) and this can account for the different change in I_{dss}. This would suggest that defects responsible for variations in V_{th} and I_{dss} are actually decoupled; a different spatial distribution of donor- and acceptor-like defects might be at the origin of this behaviour.

3.3. Output $I_{ds} - V_{ds}$ curves

Fig. 3a and b illustrate the $I_{ds} - V_{ds}$ characteristics before and after irradiation of E19 and E07 transistors, respectively. Similar results were obtained for all HD-GITs of the same type, so data of only one representative sample is shown. As can be seen from Fig. 3a–b, the variations after 5.9×10^{14} p/cm^2 in the $I_{ds} - V_{ds}$ curves are rather limited: no degradation is found in the ohmic region, while in the active (saturation) region the drain current for the same V_{ds} and V_{gs} decreases upon irradiation, and the difference between pre- and post-irradiation curves increases with increasing values of V_{ds}.

This behaviour is different from that of other proton-irradiated AlGaN/GaN HEMTs (see, for example, [62–67]), in which $I_{ds} - V_{ds}$ curves after irradiation homogeneously decreased in both the ohmic and saturation regions. In those works, the degradation is attributed to radiation-induced reduction of the 2DEG density and mobility (leading to increased sheet resistance) and, especially at lower fluences, increase in transfer resistance and contact resistivity, thus causing an increase in R_{on} and a decrease in the saturation current (hence the uniform reduction of I_{ds} in both ohmic and saturation regions of the $I_{ds} - V_{ds}$ curves). In our work, we obtained a different behaviour: we observed negligible variations in the ohmic region for both types of transistors (Fig. 3a–b); this result suggests that the transfer and sheet resistances and contact resistivity of GaN HD-GITs are only marginally affected by proton irradiation at the considered fluence. Moreover, we found a non-uniform reduction of I_{ds} in the active region, in which the difference between drain currents before and after irradiation is very small at the onset of saturation, and increases with higher V_{ds}. These results suggest that, at least at the considered fluence, a physical mechanism different from those observed in previous reports [62–67] is responsible for the degradation of the $I_{ds} - V_{ds}$ characteristics, i.e. the non-uniform decrease of I_{ds} in saturation region. We recall that, in GaN HEMTs, the onset of drain current saturation in $I_{ds} - V_{ds}$ curves occurs when V_{ds} and, consequently, the longitudinal electric field E reaches sufficiently high values leading to strong emission of longitudinal-optical (LO) phonons thus causing a degradation of electron drift velocity v_d [68]. Therefore, we believe that the increasing reduction in I_{ds} with higher V_{ds} observed upon irradiation may be attributed to a radiation-induced decrease in v_d at high electric fields. This distinctive behaviour of GaN HD-GITs with respect to previous reports may be caused by differences in device structure (particularly, in the use of a recessed p-GaN gate as opposed to Schottky gates as in [62–67]), in crystal quality as well as in fabrication methods and processing details.

More specifically, we propose the following mechanism to account for reduced v_d upon irradiation in the saturation regime. First, we recall that v_d (understood as the ensemble-average value) at steady state is linked to the momentum relaxation rate $1/\tau_m$ and to the longitudinal electric field E through the balance equation [69]:

$$v_d = \frac{e\, E\, \tau_m(T_e)}{m_e}, \tag{1}$$

where e is the electron absolute charge, m_e the electron effective mass, and T_e is the temperature of the electron population in the 2DEG channel; τ_m decreases with increasing T_e [69]. Strong emission of LO phonons at high values of E results in a large population of nonequilibrium LO phonons (*hot phonons*), which in turn induces a slowdown of the electron energy relaxation process, leading to overheating of the electron gas, and to increased momentum relaxation rate $1/\tau_m$ [69–71]. As a result, at high values of E, the differential mobility of the 2DEG decreases, i.e. the slope of the $v_d - E$ characteristic at high E decreases. We now recall that the dominant contribution to thermal conductivity of GaN at room temperature comes from acoustic phonons [72,73]. Defects induced by proton irradiation in the GaN and AlGaN layers, such as Ga vacancies [72], increase phonon scattering (i.e. the phonon relaxation rate) therein, thus leading to reduced thermal conductivity [72,73] and hence higher 2DEG temperature T_e. We justify the increase in T_e as follows. First, a reduced thermal conductivity leads to higher lattice temperature T_L in the 2DEG channel. In the hot phonon (HP) temperature approximation [71], the power dissipated per electron $P_d = e \cdot v_d \cdot E$ at steady state is equal to:

$$P_d = \hbar\omega_{LO} \cdot \frac{N(\omega_{LO}, T_{ph}) - N(\omega_{LO}, T_L)}{\tau_p}, \tag{2}$$

where $\hbar\omega_{LO}$ is the energy of LO phonons in GaN (no dispersion is assumed), τ_p is the LO phonon lifetime, and $N(\omega, T)$ is the occupation number of phonons with frequency ω at temperature T given by the Bose-Einstein distribution $N(\omega, T) = [\exp(\hbar\omega/k_B T) - 1]^{-1}$, where k_B is the Boltzmann constant. In Eq. (2), $N(\omega_{LO}, T_L)$ represents the equilibrium LO phonon occupancy, while $N(\omega_{LO}, T_{ph})$ approximates the HP

average occupancy assuming quasi-equilibrium conditions; T_{ph} is the HP temperature, approximately equal to the 2DEG temperature: $T_e \approx T_{\text{ph}}$. As can be seen from Eq. (2), if T_L increases, the same value of P_d is obtained at larger values of $N(\omega_{\text{LO}}, T_{\text{ph}})$, i.e. at higher T_e. The HP temperature approach is just an approximate model, but the same conclusions are obtained in the full quantum-mechanical framework of [70]. In this model, bulk LO phonons are replaced by interface (IF) and half-space (HS) polar-optical modes, thus accounting for the AlGaN/GaN heterostructure, so that P_d can be expressed as:

$$P_d = \frac{1}{n_{2D}A_{2D}} \sum_{\mathbf{q}} \left\{ \sum_n \left[\hbar\omega_n \frac{N(\omega_n, T_e) - g_n(\mathbf{q})}{\tau_n(\mathbf{q})} \right] + \sum_{q_z>0} \left[\hbar\omega_{LO} \frac{N(\omega_{\text{LO}}, T_e) - g_{q_z}(\mathbf{q})}{\tau_{q_z}(\mathbf{q})} \right] \right\}, \quad (3)$$

where $\mathbf{q}$ is the in-plane phonon wavevector, $g_n(\mathbf{q})$ and $g_{qz}(\mathbf{q})$ are the nonequilibrium phonon occupation numbers of IF and HS modes respectively, $1/\tau_n(\mathbf{q})$ and $1/\tau_{qz}(\mathbf{q})$ are respectively the effective phonon generation rates of IF and HS modes (which also account for phonon absorption and stimulated emission), n_{2D} is the 2DEG density, A_{2D} is the surface of the 2DEG, and $N(\omega, T)$ has the same meaning as in Eq. (2). The first addend of Eq. (3) represents the contribution of IF modes (indexed by $n = \{1,2\}$) and the second addend HS modes (indexed by the phonon wavevector in the growth direction z). IF modes have energies $\hbar\omega_n$, while HS modes have an energy $\hbar\omega_{\text{LO}}$, equal to that of bulk LO phonons; again, no dispersion is assumed. The occupation numbers $g_n(\mathbf{q})$ and $g_{qz}(\mathbf{q})$ are, respectively:

$$g_n(\mathbf{q}) = \left[\frac{N(\omega_n, T_e)}{\tau_n(\mathbf{q})} + \frac{N(\omega_n, T_L)}{\tau_p} \right] \Big/ \left[\frac{1}{\tau_n(\mathbf{q})} + \frac{1}{\tau_p} \right], \quad (4)$$

and

$$g_{q_z}(\mathbf{q}) = \left[\frac{N(\omega_{\text{LO}}, T_e)}{\tau_{q_z}(\mathbf{q})} + \frac{N(\omega_{\text{LO}}, T_L)}{\tau_p} \right] \Big/ \left[\frac{1}{\tau_{q_z}(\mathbf{q})} + \frac{1}{\tau_p} \right], \quad (5)$$

where τ_p is again the polar-optical phonon lifetime. It is straightforward to verify from Eq. (3) to (5) that, for a given T_e, P_d decreases if T_L increases, i.e. if T_L gets higher, then T_e increases as well when the same input power (i.e. P_d) is supplied to the 2DEG. Now, we recall that $1/\tau_m$ in GaN (also due to the contribution from HPs) increases with increasing T_e [69]; consequently, from Eq. (1), the drift velocity v_d (and, hence, the differential mobility) at high E is expected to further decrease upon proton irradiation due to decreased thermal conductivity (that is, increased T_e), i.e. the $v_d - E$ characteristic in the saturation region becomes even flatter due to increased electron gas self-heating with respect to pre-irradiation. This variation in the $v_d - E$ characteristics would then lead to the changes observed in the $I_{\text{ds}} - V_{\text{ds}}$ curves after irradiation. A decrease in thermal conductivity and an increase in channel temperature have been recently observed in InAlN/GaN HEMTs upon irradiation with 340 keV protons at a fluence of 5×10^{13} p/cm^2 [74], so we believe that the degradation mechanism proposed above could realistically account for a reduction of v_d at high E and hence for the observed changes in the $I_{\text{ds}} - V_{\text{ds}}$ characteristics after irradiation.

Finally, we would like to highlight that the increase in threshold voltage upon irradiation (cf. Section 3.2) can also play a role in modifying the $I_{\text{ds}} - V_{\text{ds}}$ curves of irradiated devices. Nevertheless, we believe that this contribution is actually marginal compared to the effect of the increased phonon relaxation rate. Indeed, if the increase in V_{th} was the main cause of the changes in $I_{\text{ds}} - V_{\text{ds}}$ characteristics then, after irradiation, I_{ds} would decrease not only in the saturation region but also at the saturation knee (i.e. at the intersection of the ohmic and saturation regions). However, this would not be consistent with the experimental results of Fig. 3: indeed, I_{ds} in irradiated devices decreases only after the saturation onset, while it is essentially unchanged in the ohmic region and at the saturation knee. Therefore, we believe that the observed changes in $I_{\text{ds}} - V_{\text{ds}}$ characteristics upon irradiation should be principally ascribed to a reduction in v_d at high E due to radiation-induced increase in phonon relaxation rate.

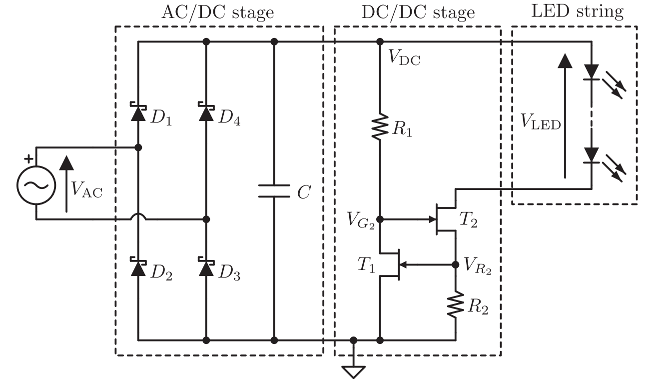

Fig. 4. Proposed linear power supply using GaN HD-GITs.

4. Power supply

By interpolating the results illustrated in the previous Section with those of Hommels et al. [26,27], we expect any variation in electrical characteristics of HD-GITs to be negligible at the target radiation levels (2.3×10^{13} n/cm^2 and 11 kGy); this demonstrates the potential of HD-GITs as candidate components for rad-hard LED power supplies for CERN tunnel lights. In order to meet the requirements on the radiation resistance, light quality and tolerance to mains voltage variations, we propose the LED power supply illustrated in Fig. 4. It comprises a single-phase diode bridge rectifier composed of 4 SiC Junction Barrier Schottky (JBS) diodes, a capacitor to smooth the rectified voltage, and a linear DC/DC regulator comprising 2 HD-GITs supplying a string of white GaN LEDs. A working prototype of the proposed power supply has been assembled, using four STPSC10H065G SiC JBS diodes from STMicroelectronics (tested against radiation in [3]) for the diode bridge, a 80 µF polypropylene capacitor, 2 Panasonic PGA26E19BA HD-GITs and two resistors R_1 and R_2 of 100 kΩ and 16 Ω, respectively; the LED string consisted of 110 Osram Oslon Square GW CSSRM2 white LEDs. This power supply is designed to operate at nominal mains voltage V_{AC} of 231 V at 50 Hz. The current of the LED string I_{LED} is given by the ratio V_{R2}/R_2, where V_{R2} is about the threshold voltage of T_1 (typically 1.2 V). The V_{ds} of T_2 accounts for the difference between the capacitor voltage V_{DC} and the voltage of the LED string V_{LED}. The values of the passive components and the number of LEDs in the string are chosen so that both transistors T_1 and T_2 operate at any instant of time in their active region for $V_{\text{AC}} \geq 220$ V (i.e. ≥95% of the nominal value); this ensures a constant DC current through the LEDs, insensitive to mains voltage fluctuations, without any light flickering. The proposed power supply is simple and intrinsically robust to radiation, as SiC JBS diodes and GaN HD-GITs exhibit variations in their electrical characteristics at radiation levels much higher than our target values, meaning that the radiation tolerance of the whole luminaire is bound to that of the LEDs (i.e. > 5 years in the typical conditions of CERN tunnel walls). Compliance with IEC 61000-3-2 standard for harmonic currents can be achieved, for example, by using an AC line filter comprising polypropylene capacitors and compact bobbin inductors, or by inserting a valley-fill circuit with voltage doubler [75] between the diode bridge and the DC/DC linear stage.

Electrical measurements have been performed on the proposed power supply with a Chauvin Arnoux CA8335 power analyser and an Agilent DSO6054A oscilloscope. The waveforms of V_{LED}, V_{DC}, V_{R2} (the voltage on R_2 resistor), and V_{G2} (the gate voltage of T_2) in the range $V_{\text{AC}} = 210 - 231$ V are shown in Fig. 5; these voltages are also

indicated in Fig. 4. In addition, Fig. 6 provides an experimental summary of the data derived from the waveforms illustrated in Fig. 5. For V_{AC} ranging from 220 V to 231 V, the measured V_{LED} is constant in time and almost insensitive to the value of V_{DC}, as illustrated in Figs. 5a–e and 6a, which shows the measured V_{LED} and the measured average V_{DC} values; as can been seen, V_{LED} only changes by 1 V from 294 V at V_{AC} = 220 V to 295 V at V_{AC} = 231 V. Consequently, the measured I_{LED} and lumen output Φ_{LED} of the LED string are also constant in time and almost unaffected by changes in V_{AC}; they respectively change from 81 mA to ≈75 mA and from 4100 lm to 3780 lm when V_{AC} goes from 220 V to 231 V (see Fig. 6b). The small increase in I_{LED} (and consequently Φ_{LED}) with decreasing values of V_{AC} is caused by the reduction in high-frequency noise (in the MHz range) superimposed on V_{R2} and V_{G2} which, as can be seen from Fig. 5a–e, depends on V_{AC} (and hence on V_{DC}): in particular, as shown in Fig. 5e, the noise amplitude steeply reduces when the instantaneous value of V_{DC} becomes lower than ≈300 V. Such reduction in high-frequency noise leads to a slight increase in the average value of V_{R2}, which therefore translates into a small increase in I_{LED} and Φ_{LED}. We attribute this noise to the non-optimal layout of the DC/DC power supply board; in the future version of the board, we will address this issue by optimizing the PCB design and by implementing suitable filters in the DC/DC stage (like e.g. a capacitor across transistor T_1). Moreover, we note that, in the considered range of V_{AC}, V_{LED} remains essentially constant in spite of the changes in I_{LED}; we attribute this insensitivity to thermal effects in the LEDs. Since in the range 220–231 V I_{LED} is constant in time, the light output is stable and without any flickering; for this reason, we define the power supply to be working in "continuous" mode for V_{AC} ≥ 220 V. The measured input active power at V_{AC} = 231 V is 24.5 W; hence, the prototype LED luminaire produces more light while absorbing less active power than a standard 36 W fluorescent tube with magnetic ballast (which typically emits 3350 lm). Despite the use of a linear topology, the efficiency η_{DC} of the DC/DC power supply is sufficiently high, with measured values higher than 89% for voltages between 220 V and 231 V (see Fig. 6c). The efficiency η_{DC} is computed as $P_{LED}/(P_{LED} + P_{loss})$, where P_{LED} is the mean value of V_{LED} × I_{LED} and

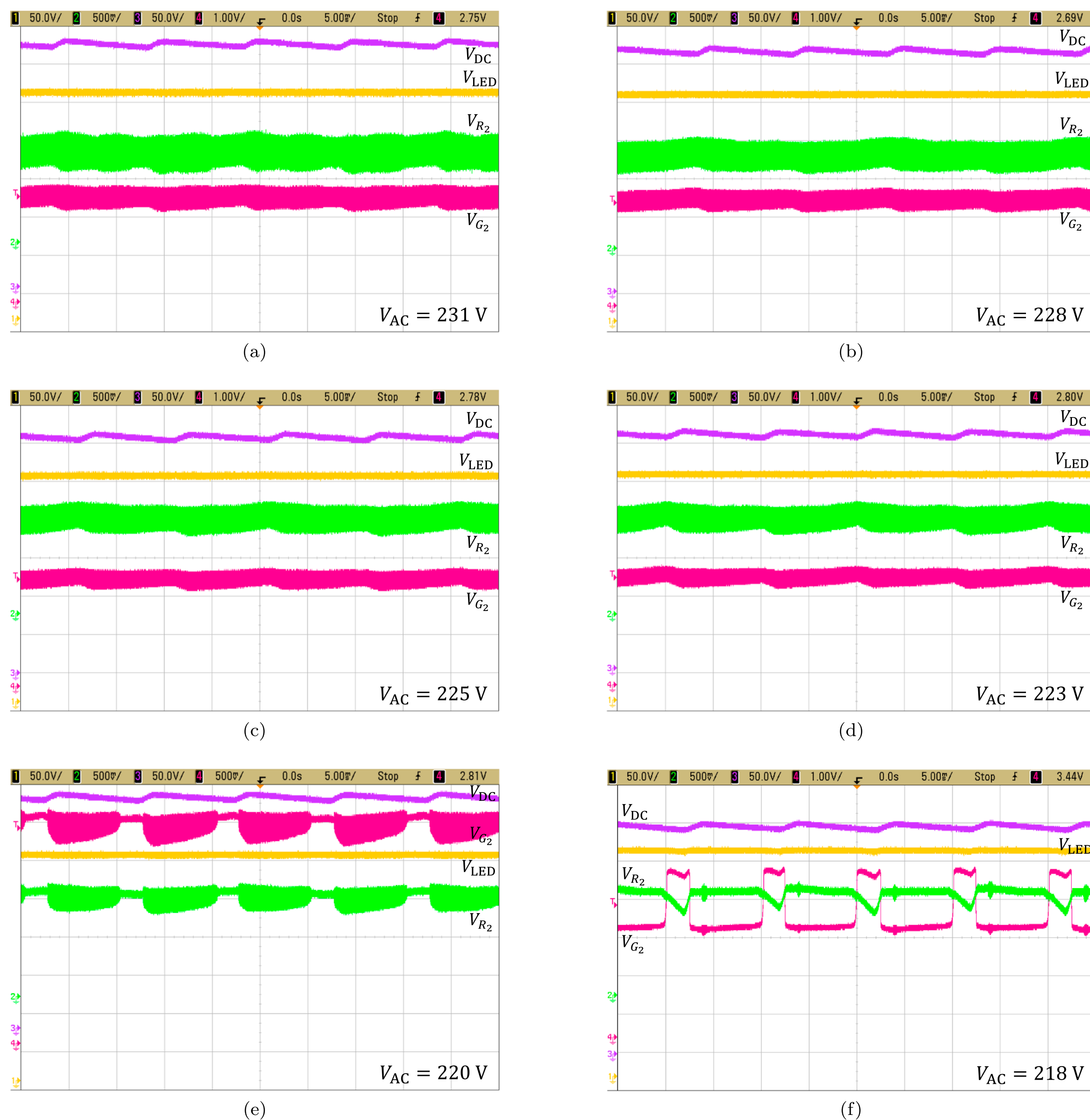

Fig. 5. Waveforms of V_{LED} (yellow traces), V_{R2} (green traces), V_{DC} (purple traces), and V_{G2} (magenta traces) at different values of V_{AC}: (a) 231 V, (b) 228 V, (c) 225 V, (d) 223 V, (e) 220 V, (f) 218 V, (g) 215 V, (h) 214 V, (i) 213 V, (j) 210 V. (For interpretation of the references to colour in this figure legend, the reader is referred to the web version of this article.)

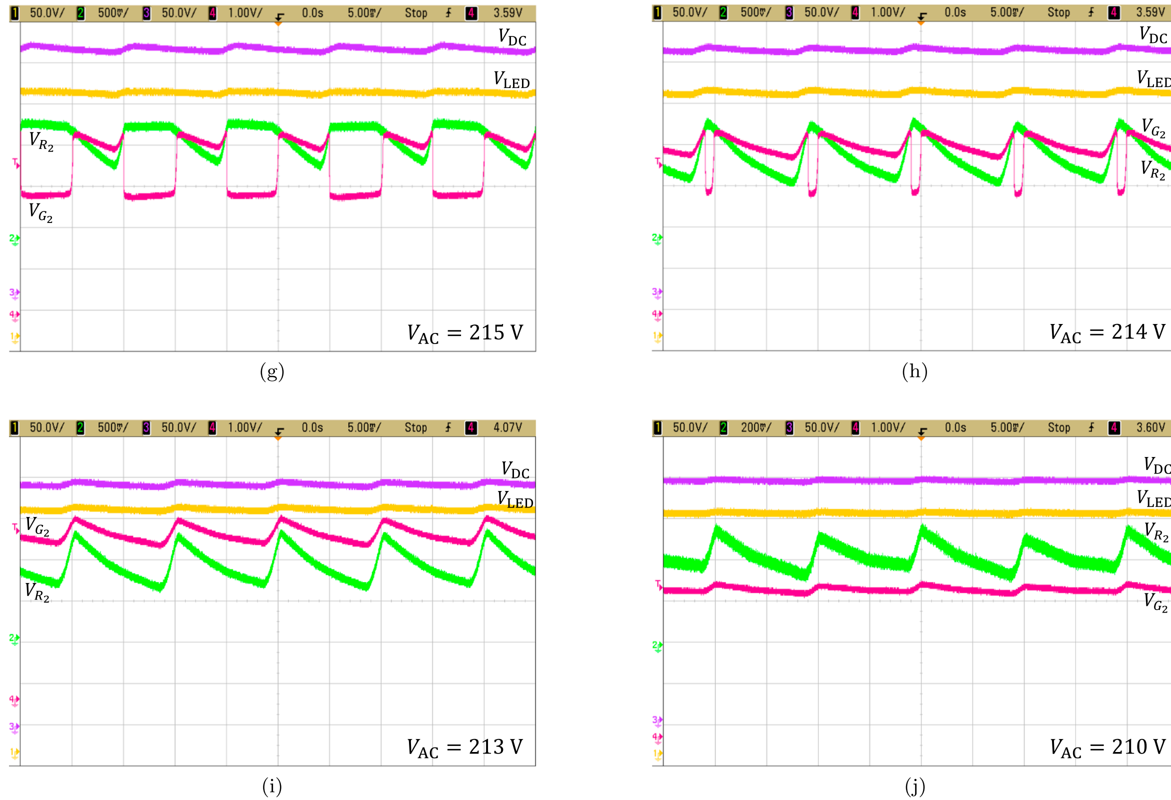

Fig. 5. (*continued*)

$P_{loss} = P_{R1} + P_{R2} + P_{T1} + P_{T2}$ is the sum of the time-averaged power losses on R_1, R_2, T_1, and T_2, respectively; these power losses are shown in Fig. 6d. In particular, the increase in η_{DC} occurring for V_{AC} from 231 V to 220 V is mostly due to the reduction in P_{T2}.

For $V_{AC} \leq 218$ V, the instantaneous value of V_{DC} becomes lower than the design value of V_{LED} (294 V) during every 10 ms cycle, and when this occurs T_1 switches off and T_2 is driven from the active to the ohmic region, resulting in a discontinuous I_{LED} and hence a 100 Hz light flickering (see Fig. 5f–j). For this reason, we term the operation regime of the DC/DC power supply for $V_{AC} \leq 218$ V as "discontinuous" mode. We note from Fig. 6b that I_{LED} reaches its maximum at $V_{AC} = 218$ V, despite not being any more constant in time (cf. V_{R2} in Fig. 5f, which presents short dips when T_1 turns off and T_2 works in ohmic region). Such further increase in I_{LED} is due to the additional reduction in high-frequency noise. Then, I_{LED} steadily decreases for $V_{AC} \leq 215$ V, as the average value of V_{R2} reduces due to the decrease in the average value of V_{DC} (cf. Fig. 6a); in particular, V_{R2} contains longer dips during each period and eventually, for $V_{AC} \leq 213$ V, T_1 is always off and T_2 works in ohmic region during the whole duration of the period (see Fig. 5g–j) with I_{LED} entirely determined by V_{DC}. From Fig. 6c, we see that η_{DC}, after reaching a maximum at 218 V, decreases for $V_{AC} \leq 215$ V. The η_{DC} maximum is caused by the further reduction in P_{T2}. The decrease in η_{DC} for lower values of V_{AC} occurs because, even if P_{T1} and P_{T2} are negligible for $V_{AC} \leq 215$ V and P_{R2} decreases due to the reduction in I_{LED}, P_{R1} still maintains high values despite the drop in V_{DC} and therefore becomes the leading term of the DC/DC power supply losses (see Fig. 6d). Consequently, for $V_{AC} \leq 215$ V, η_{DC} decreases due to the reduction in P_{LED}.

5. Conclusions

In order to evaluate their potential application as power transistors in rad-hard LED power supplies for the new lights of CERN tunnels, samples of Panasonic PGA26E19BA and PGA26E07BA HD-GITs have been irradiated with 24 GeV/c protons at a fluence of 5.9×10^{14} p/cm^2. We found only small variations in their electrical characteristics upon irradiation. For example, V_{th} increases on average only by $\approx$11–13 mV after irradiation, due to negatively charged traps induced by proton bombardment. I_{dss} increases on average by 25–30% upon irradiation due to increased defect density, thus enhancing hopping and thermally assisted multistep tunnelling conduction between the electrodes. The $I_{ds} - V_{ds}$ curves of both types of HD-GITs do not show any variation in R_{on} and highlight a decrease in I_{ds} at high V_{ds}, which should be caused by reduced electron drift velocity at high electric fields due to radiation-induced increase in phonon relaxation rate. In summary, GaN HD-GITs present only limited variations in their electrical properties after a fluence > 10 times larger than the LED lifetime. Finally, we proposed a rad-hard LED power supply for lighting of CERN tunnels using HD-GITs as power transistors, capable of meeting the requirements in terms of light quality; the radiation tolerance of the proposed lighting system is essentially bound to that of the LEDs, thanks to an accurate selection of its semiconductor components.

CRediT authorship contribution statement

Alessandro Floriduz: Conceptualization, Methodology, Software, Validation, Investigation, Writing - original draft, Visualization. **James D. Devine:** Supervision, Project administration.

Declaration of competing interest

The authors declare that they have no known competing financial interests or personal relationships that could have appeared to influence the work reported in this paper.

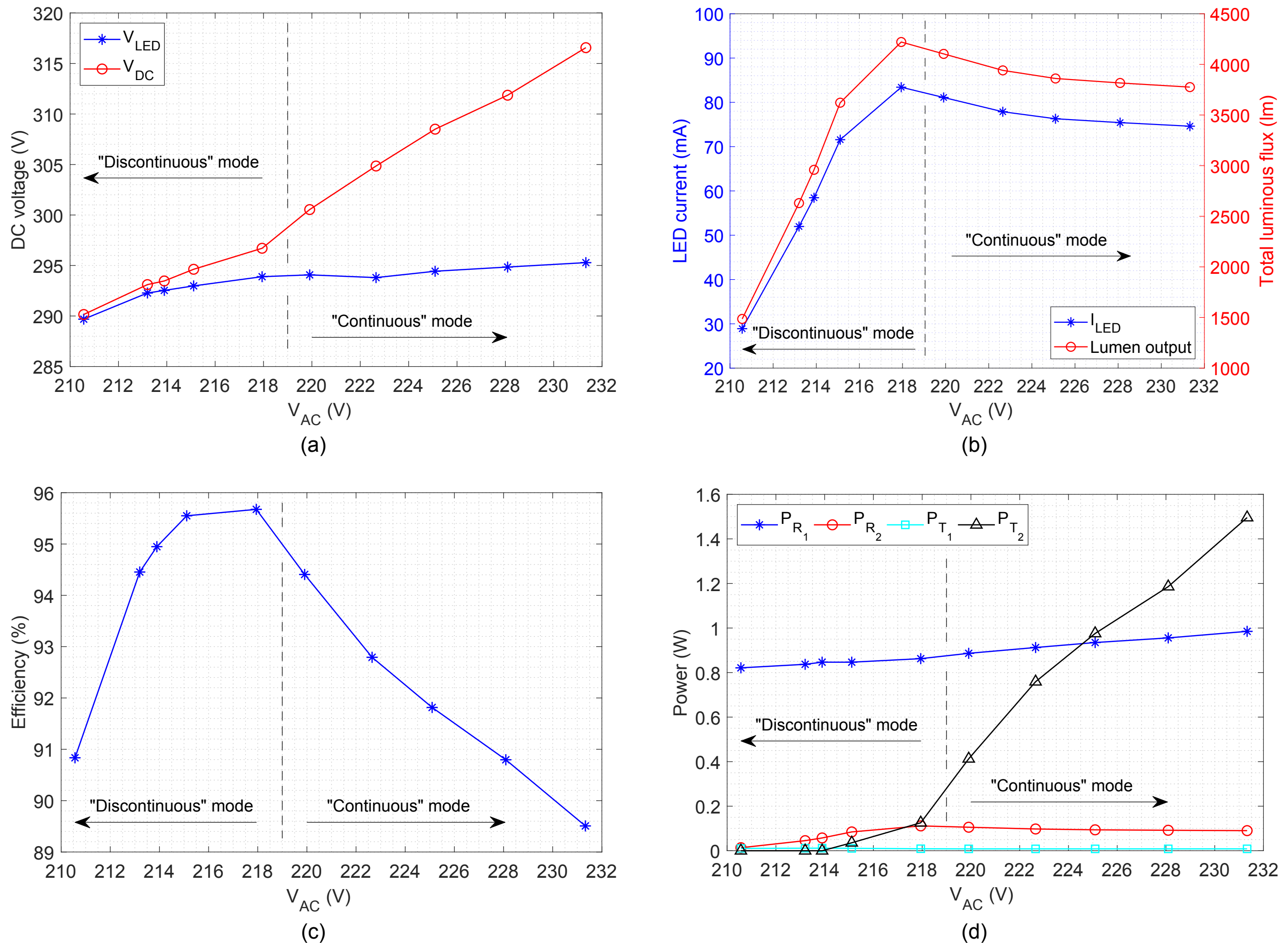

Fig. 6. Dependence on V_{AC} of: (a) the measured V_{LED} and measured average V_{DC}; (b) the average LED current I_{LED} and total luminous flux Φ_{tot}; (c) the efficiency of the DC/DC power supply; (d) the power dissipation of the elements in the DC/DC power supply. In each plot, the intervals $V_{AC} \leq 218$ V and $V_{AC} \geq 220$ V corresponding, respectively, to the "discontinuous" and "continuous" operation modes of the DC/DC power supply are indicated. All values presented in this Figure are derived from the measured waveforms shown in Fig. 5.

Acknowledgements

The authors thankfully acknowledge Ayanori Ikoshi, Shuichi Urashima, and Francois Perraud from Panasonic for insightful discussions. They also gratefully thank Giuseppe Pezzullo, Georgi Gorine, Isidre Mateu, and Federico Ravotti (CERN) for sample irradiation and assistance at IRRAD facility, and Eva Cano Gonzalez (CERN) for help with prototype power supply measurements.

This research did not receive any specific grant from funding agencies in the public, commercial, or not-for-profit sectors.

References

[1] J.P. De Carvalho Saraiva, M. Brugger, Radiation environments and their impact at the CERN's injector chain, Tech. Rep. CERN-ACC-NOTE-2015-0042, http://cds.cern.ch/record/2114889 (Dec 2015).

[2] A. Floriduz, J.D. Devine, Modelling of proton irradiated GaN-based high-power white light-emitting diodes, Jpn. J. Appl. Phys. 57 (8) (2018) 080304, , https://doi.org/10.7567/JJAP.57.080304.

[3] A. Floriduz, J.D. Devine, Radiation testing of optical and semiconductor components for radiation-tolerant LED luminaires, Presented at the 18th Eur. Conf. Radiat. Effects on Components and Systems (RADECS), Sept 2018.

[4] J.D. Devine, A. Floriduz, Radiation hardening of LED luminaires for accelerator tunnels, Proc. 16th Eur. Conf. Radiat. Effects on Components and Systems (RADECS), 2016, pp. 1–6, , https://doi.org/10.1109/RADECS.2016.8093210.

[5] S.Y. Hui, S.N. Li, X.H. Tao, W. Chen, W.M. Ng, A novel passive offline LED driver with long lifetime, IEEE Trans. Power Electron. 25 (10) (2010) 2665–2672, https://doi.org/10.1109/TPEL.2010.2048436.

[6] L.Z. Scheick, L.E. Selva, Effect of dose history on SEGR properties of power MOSFETs, IEEE Trans. Nucl. Sci. 54 (6) (2007) 2568–2575, https://doi.org/10.1109/TNS.2007.910127.

[7] A. Akturk, J.M. McGarrity, S. Potbhare, N. Goldsman, Radiation effects in commercial 1200 V 24 A silicon carbide power MOSFETs, IEEE Trans. Nucl. Sci. 59 (6) (2012) 3258–3264, https://doi.org/10.1109/TNS.2012.2223763.

[8] S.J. Pearton, F. Ren, E. Patrick, M.E. Law, A.Y. Polyakov, Ionizing radiation damage effects on GaN devices, ECS J. Solid State Sci. Technol. 5 (2) (2016) Q35–Q60, https://doi.org/10.1149/2.0251602jss.

[9] Transphorm, Transphorm GaN vs. e-mode, https://www.transphormusa.com/en/document/transphorm-vs-emode/.

[10] P. Brohlin, Y.K. Ramadass, C. Kaya, Direct-drive configuration for GaN devices, Texas Instruments white paper (SLPY008), http://www.ti.com/lit/wp/slpy008a/slpy008a.pdf, (Nov 2018).

[11] N. Kaneko, et al., Normally-off AlGaN/GaN HFETs using NiO_x gate with recess, Proc. 21st Int. Symp. Power Semicond. Devices & IC's (ISPSD), IEEE, 2009, pp. 25–28, , https://doi.org/10.1109/ISPSD.2009.5157992.

[12] A. Lidow, A. Nakata, M. Rearwin, J. Strydom, A.M. Zafrani, Single-event and radiation effect on enhancement mode gallium nitride FETs, Proc. 2014 IEEE Radiat. Effects Data Workshop (REDW), IEEE, 2014, pp. 1–7, , https://doi.org/10.1109/REDW.2014.7004594.

[13] Di Maso, D. Chen, System level considerations with GaN power switching, in: Presented at the IEEE Appl. Power Electron. Conf. Expo. (APEC), San Antonio, TX, USA, https://gansystems.com/wp-content/uploads/2018/04/APEC18-System-Level-Considerations-with-GaN-Power-Switching.pdf (Mar 2018).

[14] D. Kinzer, S. Oliver, Monolithic HV GaN power ICs: performance and application, IEEE Power Electron. Mag. 3 (3) (2016) 14–21, https://doi.org/10.1109/MPEL.2016.2585474.

[15] Panasonic, GaN power transistors, White paper rev. 1.0, https://eu.industrial.panasonic.com/sites/default/pidseu/files/pan_18047_whitepaper_gan_web.pdf, (2018).

[16] D.M. Keum, H.-K. Sung, H. Kim, Degradation characteristics of normally-off p-AlGaN gate AlGaN/GaN HEMTs with 5 MeV proton irradiation, IEEE Trans. Nucl. Sci. 64 (1) (2017) 258–262, https://doi.org/10.1109/TNS.2016.2612227.

[17] D. Wellekens, et al., Architecture choice for radiation-hard AlGaN/GaN HEMT power devices, Proc. 17th Eur. Conf. Radiat. Effects on Components and Systems (RADECS), IEEE, 2017, pp. 1–5, , https://doi.org/10.1109/RADECS.2017.8696192.

[18] P. Parikh, et al., 650 volt GaN commercialization reaches automotive standards, ECS Trans. 80 (7) (2017) 17–28, https://doi.org/10.1149/08007.0017ecst.
[19] X. Wan, et al., Low energy proton irradiation effects on commercial enhancement mode GaN HEMTs, IEEE Trans. Nucl. Sci. 64 (1) (2017) 253–257, https://doi.org/10.1109/TNS.2016.2621065.
[20] S. Dhawan, et al., Buck converter development for the inner detector environment of the sLHC upgrade, https://shaktipower.sites.yale.edu/sites/default/files/files/DC-DC_Paper_To_be_Published.pdf, (2011).
[21] A. Lidow, K. Smalley, Radiation tolerant enhancement mode gallium nitride (eGaN™) FET characteristics, Proc. GOMAC Tech Conf., Las Vegas, Nevada, 2012 https://epc-co.com/EPC/Portals/0/epc/documents/papers/GOMAC%20Paper%202012.pdf.
[22] C. Abbate, et al., Radiation performance of new semiconductor power devices for the LHC experiment upgrades, Proc. Sci. (2013) 1–7, https://doi.org/10.22323/1.189.0007.
[23] A. Lidow, J. Strydom, M. Rearwin, Radiation tolerant enhancement-mode gallium nitride FETs for high frequency DC-DC conversion, Proc. GOMAC Tech Conf, 2014, pp. 1–4 https://epc-co.com/epc/Portals/0/epc/documents/papers/Radiation%20Tolerant%20eGaN%20FETs%20for%20High%20Frequency%20DC-DC%20Conversion.pdf.
[24] A. Durier, A. Bensoussan, M. Zerarka, C. Ghfiri, A. Boyer, H. Frémont, A methodologic project to characterize and model COTS component reliability, Microelectron. Reliab. 55 (9–10) (2015) 2097–2102 https://doi.org/10.1016/j.microrel.2015.06.140.
[25] L.Z. Scheick, Recent gallium nitride power HEMT single-event testing results, Proc. 2016 IEEE Radiat. Effects Data Workshop (REDW), IEEE, 2016, pp. 1–6, , https://doi.org/10.1109/NSREC.2016.7891731.
[26] B. Hommels, et al., High-voltage multiplexing for ATLAS ITk, tech. Rep. ATL-COM-ITK-2017-048, http://cds.cern.ch/record/2291391, (2017).
[27] D. Lynn, et al., Radiation hard GaNFET high voltage multiplexing (HV Mux) for the ATLAS upgrade silicon strip tracker, tech. Rep. ATL-COM-ITK-2017-026, http://cds.cern.ch/record/2286244, (2017).
[28] M. Zerarka, O. Crepel, Radiation robustness of normally-off GaN/HEMT power transistors (COTS), Microelectron. Reliab. 88 (2018) 984–991, https://doi.org/10.1016/j.microrel.2018.07.148.
[29] P.J. Martínez, E. Maset, D. Gilabert, E. Sanchis-Kilders, J.B. Ejea, Evidence of dynamic-R_{on} degradation on low-dose ^{60}Co gamma radiation AlGaN/GaN HEMTs, Semicond. Sci. Technol. 33 (11) (2018) 115017, , https://doi.org/10.1088/1361-6641/aae616.
[30] E. Mizuta, et al., Single-event damage observed in GaN-on-Si HEMTs for power control applications, IEEE Trans. Nucl. Sci. 65 (8) (2018) 1956–1963, https://doi.org/10.1109/TNS.2018.2819990.
[31] K. Tanaka, H. Umeda, H. Ishida, M. Ishida, T. Ueda, Effects of hole traps on the temperature dependence of current collapse in a normally-OFF gate-injection transistor, Jpn. J. Appl. Phys. 55 (5) (2016) 054101, , https://doi.org/10.7567/jjap.55.054101.
[32] M. Yanagihara, Y. Uemoto, T. Ueda, T. Tanaka, D. Ueda, Recent advances in GaN transistors for future emerging applications, Phys. Status Solidi A 206 (6) (2009) 1221–1227, https://doi.org/10.1002/pssa.200880968.
[33] H. Okita, et al., Through recess and regrowth gate technology for realizing process stability of GaN-based gate injection transistors, IEEE Trans. Electron Devices 64 (3) (2017) 1026–1031, https://doi.org/10.1109/TED.2017.2653847.
[34] S. Kaneko, et al., Current-collapse-free operations up to 850 V by GaN-GIT utilizing hole injection from drain, Proc. 27th Int. Symp. Power Semicond. Devices & IC's (ISPSD), IEEE, 2015, pp. 41–44, , https://doi.org/10.1109/ISPSD.2015.7123384.
[35] K. Tanaka, et al., Reliability of hybrid-drain-embedded gate injection transistor, Proc. 2017 IEEE Int. Reliab. Phys. Symp. (IRPS), IEEE, 2017, pp. 4B–2, , https://doi.org/10.1109/IRPS.2017.7936308.
[36] F. Ravotti, B. Gkotse, M. Glaser, IRRAD: The new 24 GeV/c proton irradiation facility at CERN, Proc. 12th Int. Topical Meeting Nucl. Appl. Accel. (AccApp '15), 2015, pp. 10–13 http://cds.cern.ch/record/2237333.
[37] I. Mateu, M. Moll, E. Curras, F. Ravotti, H. Neugebauer, M. Glaser, NIEL hardness factor determination for the new proton irradiation facility at CERN, tech. Rep. AIDA-2020-SLIDE-2016-002, http://cds.cern.ch/record/2162852, (2016).
[38] F. Ravotti, Private communication (2019).
[39] S.J. Pearton, R. Deist, F. Ren, L. Liu, A.Y. Polyakov, J. Kim, Review of radiation damage in GaN-based materials and devices, J. Vac. Sci. Technol. A 31 (5) (2013) 050801, , https://doi.org/10.1116/1.4799504.
[40] T. Roy, et al., Process dependence of proton-induced degradation in GaN HEMTs, IEEE Trans. Nucl. Sci. 57 (6) (2010) 3060–3065, https://doi.org/10.1109/TNS.2010.2073720.
[41] A. Sasikumar, et al., Proton irradiation-induced traps causing V_T instabilities and RF degradation in GaN HEMTs, Proc. 2015 IEEE Int. Reliab. Phys. Symp. (IRPS), IEEE, 2015, pp. 2E–3, , https://doi.org/10.1109/IRPS.2015.7112688.
[42] M.J. Uren, M. Cäsar, M.A. Gajda, M. Kuball, Buffer transport mechanisms in intentionally carbon doped GaN heterojunction field effect transistors, Appl. Phys. Lett. 104 (26) (2014) 263505, , https://doi.org/10.1063/1.4885695.
[43] A. Pérez-Tomás, et al., Analysis of the AlGaN/GaN vertical bulk current on Si, sapphire, and free-standing GaN substrates, J. Appl. Phys. 113 (17) (2013) 174501, , https://doi.org/10.1063/1.4803130.
[44] F. Gao, S.C. Tan, J.A. del Alamo, C.V. Thompson, T. Palacios, Impact of water-assisted electrochemical reactions on the OFF-state degradation of AlGaN/GaN HEMTs, IEEE Trans. Electron Devices 61 (2) (2013) 437–444, https://doi.org/10.1109/TED.2013.2293114.
[45] M.J. Uren, et al., Intentionally carbon-doped AlGaN/GaN HEMTs: necessity for vertical leakage paths, IEEE Electron Device Lett. 35 (3) (2014) 327–329, https://doi.org/10.1109/LED.2013.2297626.
[46] M.J. Uren, et al., "Leaky dielectric" model for the suppression of dynamic R_{ON} in carbon-doped AlGaN/GaN HEMTs, IEEE Trans. Electron Devices 64 (7) (2017) 2826–2834, https://doi.org/10.1109/TED.2017.2706090.
[47] W. Zhang, E. Simoen, M. Zhao, J. Zhang, Analysis of leakage mechanisms in AlN nucleation layers on p-Si and p-SOI substrates, IEEE Trans. Electron Devices 66 (4) (2019) 1849–1855, https://doi.org/10.1109/TED.2019.2899964.
[48] X. Li, et al., Investigation on carrier transport through AlN nucleation layer from differently doped Si(111) substrates, IEEE Trans. Electron Devices 65 (5) (2018) 1721–1727, https://doi.org/10.1109/TED.2018.2810886.
[49] X. Li, et al., Buffer vertical leakage mechanism and reliability of 200-mm GaN-on-SOI, IEEE Trans. Electron Devices 66 (1) (2018) 553–560, https://doi.org/10.1109/TED.2018.2878457.
[50] L. Sayadi, et al., The role of silicon substrate on the leakage current through GaN-on-Si epitaxial layers, IEEE Trans. Electron Devices 65 (1) (2017) 51–58, https://doi.org/10.1109/TED.2017.2773670.
[51] J.D. Greenlee, et al., Degradation mechanisms of 2 MeV proton irradiated AlGaN/GaN HEMTs, Appl. Phys. Lett. 107 (8) (2015) 083504, , https://doi.org/10.1063/1.4929583.
[52] V.F. Gantmakher, Electrons and Disorder in Solids, No. 130 in International Series of Monographs on Physics, Oxford University Press, 2005, https://doi.org/10.1093/acprof:oso/9780198567561.001.0001.
[53] D. Mahaveer Sathaiya, S. Karmalkar, Thermionic trap-assisted tunneling model and its application to leakage current in nitrided oxides and AlGaN/GaN high electron mobility transistors, J. Appl. Phys. 99 (9) (2006) 093701, , https://doi.org/10.1063/1.2191620.
[54] L. Larcher, Statistical simulation of leakage currents in MOS and flash memory devices with a new multiphonon trap-assisted tunneling model, IEEE Trans. Electron Devices 50 (5) (2003) 1246–1253, https://doi.org/10.1109/TED.2003.813236.
[55] W.R. Harrell, C. Gopalakrishnan, Implications of advanced modeling on the observation of Poole–Frenkel effect saturation, Thin Solid Films 405 (1–2) (2002) 205–217, https://doi.org/10.1016/S0040-6090(01)01752-7.
[56] Panasonic, PGA26E19BA Datasheet, (Jan 2017).
[57] Panasonic, PGA26E07BA Datasheet, (Jan 2017).
[58] Z. Zhang, et al., Correlation of proton irradiation induced threshold voltage shifts to deep level traps in AlGaN/GaN heterostructures, J. Appl. Phys. 119 (16) (2016) 165704, , https://doi.org/10.1063/1.4948298.
[59] Y.S. Puzyrev, T. Roy, E.X. Zhang, D.M. Fleetwood, R.D. Schrimpf, S.T. Pantelides, Radiation-induced defect evolution and electrical degradation of AlGaN/GaN high-electron-mobility transistors, IEEE Trans. Nucl. Sci. 58 (6) (2011) 2918–2924, https://doi.org/10.1109/TNS.2011.2170433.
[60] G. Cellere, L. Larcher, M.G. Valentini, A. Paccagnella, Micro breakdown in small-area ultrathin gate oxides, IEEE Trans. Electron Devices 49 (8) (2002) 1367–1374, https://doi.org/10.1109/TED.2002.801443.
[61] N.F. Mott, W.D. Twose, The theory of impurity conduction, Adv. Phys. 10 (38) (1961) 107–163, https://doi.org/10.1080/00018736100101271.
[62] Y. Xi, et al., Effect of 5 MeV proton radiation on DC performance and reliability of circular-shaped AlGaN/GaN high electron mobility transistors, J. Vac. Sci. Technol. B 32 (1) (2014) 012201, , https://doi.org/10.1116/1.4836577.
[63] B. Luo, et al., DC and RF performance of proton-irradiated AlGaN/GaN high electron mobility transistors, Appl. Phys. Lett. 79 (14) (2001) 2196–2198, https://doi.org/10.1063/1.1408606.
[64] B.D. White, et al., Electrical, spectral, and chemical properties of 1.8 MeV proton irradiated AlGaN/GaN HEMT structures as a function of proton fluence, IEEE Trans. Nucl. Sci. 50 (6) (2003) 1934–1941, https://doi.org/10.1109/TNS.2003.821827.
[65] A.P. Karmarkar, et al., Proton irradiation effects on GaN-based high electron-mobility transistors with Si-doped $Al_xGa_{1-x}N$ and thick GaN cap layers, IEEE Trans. Nucl. Sci. 51 (6) (2004) 3801–3806, https://doi.org/10.1109/TNS.2004.839199.
[66] L. Liu, et al., Study on the effects of proton irradiation on the dc characteristics of AlGaN/GaN high electron mobility transistors with source field plate, J. Vac. Sci. Technol. B 32 (2) (2014) 022202, , https://doi.org/10.1116/1.4866401.
[67] B.D. White, et al., Characterization of 1.8-MeV proton-irradiated AlGaN/GaN field-effect transistor structures by nanoscale depth-resolved luminescence spectroscopy, IEEE Trans. Nucl. Sci. 49 (6) (2002) 2695–2701, https://doi.org/10.1109/TNS.2002.805427.
[68] M. Li, Y. Wang, 2-D analytical model for current–voltage characteristics and transconductance of AlGaN/GaN MODFETs, IEEE Trans. Electron Devices 55 (1) (2008) 261–267, https://doi.org/10.1109/TED.2007.911076.
[69] J. Khurgin, Y.J. Ding, D. Jena, Hot phonon effect on electron velocity saturation in GaN: a second look, Appl. Phys. Lett. 91 (25) (2007) 252104, , https://doi.org/10.1063/1.2824872.
[70] J.-Z. Zhang, A. Dyson, B.K. Ridley, Hot electron energy relaxation in lattice-matched InAlN/AlN/GaN heterostructures: the sum rules for electron-phonon interactions and hot-phonon effect, J. Appl. Phys. 117 (2) (2015) 025701, , https://doi.org/10.1063/1.4905717.
[71] A. Matulionis, et al., Hot-phonon temperature and lifetime in a biased $Al_xGa_{1-x}N$/GaN channel estimated from noise analysis, Phys. Rev. B 68 (3) (2003) 035338, , https://doi.org/10.1103/PhysRevB.68.035338.
[72] L. Lindsay, D.A. Broido, T.L. Reinecke, Thermal conductivity and large isotope effect in GaN from first principles, Phys. Rev. Lett. 109 (9) (2012) 095901, , https://doi.org/10.1103/PhysRevLett.109.095901.
[73] J. Zou, D. Kotchetkov, A.A. Balandin, D.I. Florescu, F.H. Pollak, Thermal conductivity of GaN films: effects of impurities and dislocations, J. Appl. Phys. 92 (5) (2002) 2534–2539, https://doi.org/10.1063/1.1497704.
[74] T. Anderson, et al., Effect of proton irradiation on thermal resistance and breakdown voltage of InAlN/GaN high electron mobility transistors, J. Vac. Sci. Technol. B 32 (5) (2014) 051203, , https://doi.org/10.1116/1.4891629.
[75] K.K. Sum, Improved valley-fill passive current shaper, Proc. Power Syst. World, Citeseer, 1997, pp. 1–8 https://www.coilws.com/Publications/ImprVF.pdf.